Origin of coherent phonons in Bi_2Te_3 excited by ultrafast laser pulses

Yaguo Wang,[*,†] Liang Guo,[†] and Xianfan Xu[‡]
School of Mechanical Engineering and Birck Nanotechnology Center, Purdue University, West Lafayette, Indiana 47907, USA

Jonathan Pierce
Center for Solid State Energetics, RTI International, Research Triangle Park, North Carolina 27709, USA

Rama Venkatasubramanian
Johns Hopkins University, Applied Physics Laboratory, Laurel, Maryland 20723, USA
(Received 9 February 2013; revised manuscript received 31 May 2013; published 26 August 2013)

Femtosecond laser pulses are used to excite coherent optical phonons in single crystal Bi_2Te_3 thin films. Oscillations from low- and high-frequency A_{1g} phonon modes are observed. A perturbation model based on molecular dynamics reveals various possibilities of phonon generation due to complex interactions among different phonon modes. In order to elucidate the process of phonon generation, measurements on thin films with thicknesses below the optical absorption depth are carried out, showing that a gradient force is necessary to excite the observed A_{1g} phonon modes, which provides a refined picture of displacive excitation of coherent phonon.

DOI: 10.1103/PhysRevB.88.064307 PACS number(s): 63.20.D−, 78.66.−w, 63.20.dd, 78.47.J−

Bismuth telluride (Bi_2Te_3) has been an important semiconductor thermoelectric material. Bulk Bi_2Te_3 possesses a thermoelectric figure of merit (ZT) of about 1.0, while ZT of Bi_2Te_3/Sb_2Te_3 superlattice was reported as high as 2.4 (see Ref. 1). The recent discovery of Bi_2Te_3 thin films as a topological insulator has drawn new interest.[2] One of the material's fundamentals is the excitation of energy carriers and interactions among energy carriers including photons, electrons, and phonons. Femtosecond time-resolved phonon spectroscopy is a powerful technique for investigating phonon dynamics. The ability to generate and control coherent phonon oscillations using optical pulses has triggered interests in the study of semimetals,[3–6] transition metals,[7] semiconductors,[8–11] superlattices,[12] semi-insulators,[13] and resonant interactions between filled atoms and cage lattice.[14] For many materials, knowing phonon excitation and interaction processes is vital for the investigation of transport properties.

It has been generally established that in absorbing materials, coherent phonon is excited through a displacive excitation of coherent phonon (DECP) process,[15] which was considered to be a special case of impulsive stimulated Raman scattering (ISRS).[16,17] For absorbing materials, the laser energy is first coupled into electrons. If the equilibrium positions of ions are altered by hot electrons or the electric field, the ions would oscillate coherently around their new equilibrium positions. This coherent vibration can be detected using time-resolved optical measurements. Even though DECP and ISRS have been accepted in most literatures, some specific phonon-excitation processes have also been suggested. Boschetto *et al.*[18] and Garl *et al.*[19] indicated that the polarization force exerted by the laser electric field, the ponderomotive force which originates from the nonuniform oscillating electric field, and the thermal force caused by the spatial gradient of the temperature difference between hot electrons and the cold lattice can be responsible for the coherent phonon generation in Bi. Therefore, the processes of phonon generation and the resulting complex phonon oscillation are still a subject of discussion.

In this paper, we employ femtosecond time-resolved phonon spectroscopy to investigate coherent phonon dynamics in single-crystal Bi_2Te_3 thin films. Excitation of low- and high-frequency optical phonons is observed. A perturbation model based on molecular dynamic (MD) simulation is developed to explain the interactions among the phonon modes. The combined MD studies and the phonon spectroscopy on single-crystal films with thicknesses ranging from a few nm to hundreds of nm reveal phonon interactions and the driving forces for coherent phonon excitation.

All experiments were performed in a collinear two-color (400 nm and 800 nm) pump-probe scheme. The laser pulses have 100 fs full width at half maximum pulse width, 800 nm center wavelength, and repetition rate of 5 kHz. A second harmonic crystal is used to generate pump pulses at 400 nm. The pump and the probe beams are focused onto the sample at normal direction with diameters of 80 and 20 μm and fluence of about 0.25 mJ/cm^2 and 0.02 mJ/cm^2, respectively. The samples are c-plane orientated single crystalline Bi_2Te_3 thin films grown via metal-organic chemical-vapor deposition on GaAs (100) substrates.[20] The penetration depths for 400 nm and 800 nm are about 9.1 nm and 10.0 nm calculated by data in (Ref. 21), so the entire excited region is probed. We also tested using an 800-nm pump and a 720-nm probe, which led to similar results. The thickness of the samples ranges from 1.0 μm to 5 nm.

Bulk Bi_2Te_3 has a rhombohedral primitive cell in space group $R\bar{3}m$, and the corresponding conventional unit cell is hexagonal, consisting of periodically arranged fivefold stacks along the c axis: TeI–Bi–TeII–Bi–TeI.[22] The five atoms in each primitive unit cell give three acoustic phonon modes and twelve optical phonon modes. The twelve optical modes are two A_{1g} and two E_g (Raman active), and two A_{1u} and two E_u modes (IR active). Only eight modes are counted here due to the degeneracy of the transverse modes.[22] Figure 1 illustrates the corresponding atomic displacements for these modes. For MD simulations, we employ two-body potentials that are derived from the density-functional theory and have been implemented in MD to calculate the bulk lattice

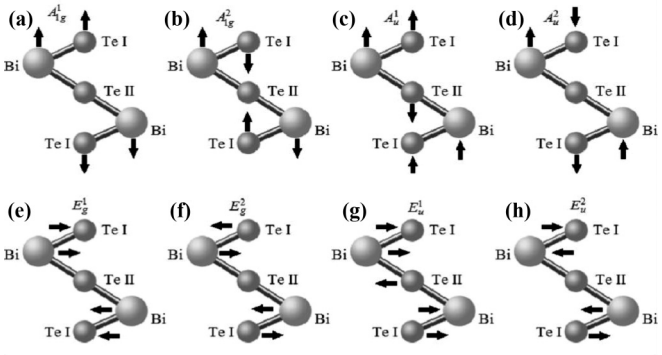

FIG. 1. Optical phonon modes in Bi_2Te_3.

thermal conductivity[23] and the mode-wise lattice thermal conductivity.[24] The two-body potential is used together with the Wolf's summation[25] to evaluate the long-range Coulomb interaction. Small perturbations are introduced to the molecular system by slightly displacing the atomic positions along the directions indicated in Fig. 1. For example, the A^1_{1g} phonon mode is generated in MD by stretching the two pairs of Bi and TeI atoms away from the center along the c axis. In this calculation, the stretching distance is about 2% of the nearest-bond distance. The temperature rise caused by this perturbation is about 8 K from an initial temperature of 300 K. This is equivalent to a laser fluence of about 0.03 mJ/cm^2. The atoms are then released to allow for vibrations determined by the interatomic potentials, which reflects the phonon dephasing and interaction processes. The phonon frequencies obtained from the calculation can then be compared with the experimental data.

Figure 2 shows the experimentally observed oscillations from the 1-μm-thick Bi_2Te_3 film. The optical signal consists of a nonoscillatory background, the initial drop, and a slow recovery, which is related to electron excitation and lattice heating via electron-lattice coupling and oscillatory components appearing right after laser excitation. Our previous study has shown that the dominant phonon oscillation is the A^1_{1g} phonon mode.[26] For the oscillation patterns in Fig. 2, a Fast Fourier Transform (FFT) of the data reveals fast and slow oscillations at 3.91 THz and 1.82 THz, corresponding to the frequencies of A^2_{1g} and A^1_{1g} phonon modes with a slight red shift compared with the Raman measurements (Table I). We consider these two phonon oscillation modes and employ the

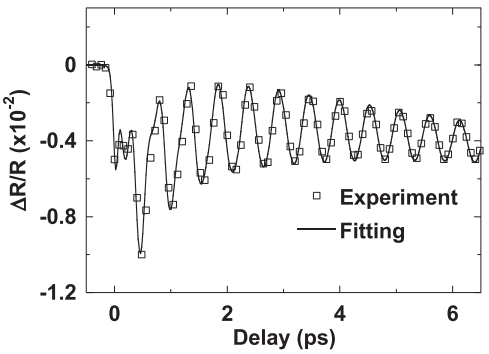

FIG. 2. Coherent phonons excited by femtosecond laser pulses (dots) in the 1-μm-thick Bi_2Te_3 film and the fitting result (solid line).

TABLE I. Comparison of phonon frequencies from Raman and IR spectroscopy, femtosecond time-resolved spectroscopy, and MD simulation. All units are in THz.

Mode	Raman (Refs. 22 and 27)	IR (Ref. 22)	Femtosecond spectroscopy	MD simulation
A^1_{1g}	1.88		1.82	1.84
A^2_{1g}	4.02		3.91	3.74
A^1_{1u}		2.82		2.88
A^2_{1u}		3.60		3.58
E^1_g	1.1			1.47
E^2_g	3.09			3.42
E^1_u		1.50		1.43
E^2_u		2.85		2.90

model below to fit the reflectivity signal:

$$R_{\text{total}} = A_e e^{-\frac{t}{\tau_e}} + A_L e^{+\frac{t}{\tau_L}} + A_{pf} e^{-\frac{t}{\tau_{pf}}} \cos[(\Omega_{pf} + \beta_{pf} t)t + \varphi_{pf}] + A_{ps} e^{-\frac{t}{\tau_{ps}}} \cos[(\Omega_{ps} + \beta_{ps} t)t + \varphi_{ps}]. \quad (1)$$

Equation (1) represents the total reflectivity response R_{total} from electron relaxation (e), lattice heating (L), fast phonon mode (pf), and slow phonon mode (ps), respectively. A is the amplitude of reflectivity change. τ denotes the time constant (the decay time) of each process. Ω, β, and φ stand for phonon angular frequency, chirping coefficient, and initial phase of phonon vibration, respectively. Taking into account the finite pulse width of the pump and the probe pulses, the total response is convoluted with the experimentally determined cross-correlation of pump and probe pulses, $G_{\text{cross-correlation}}$, giving $F = R_{\text{total}} \otimes G_{\text{cross-correlation}}$, which is used to fit the experimental data. The solid curve in Fig. 2 shows that a good fit can be obtained.

MD calculations produced frequencies of all the phonon modes, including IR active modes, which are all in close agreement with the Raman or IR measurement data, as summarized in Table I. Moreover, MD calculations reveal interactions among different phonon modes. Figures 3(a) and 3(b) show the transient atomic displacements of TeI atoms for excitation of A^1_{1g} and A^2_{1g} mode, respectively. The corresponding FFT spectra are shown in Figs. 3(c) and 3(d). It is seen that for the case of A^1_{1g} phonon excitation, coherent A^2_{1g} phonons are also generated and vice versa. Phonon dephasing times are also computed. When the A^1_{1g} mode is excited, the dephasing time for A^1_{1g} and A^2_{1g} phonons are about 12 ps and 4 ps, respectively. From experiments, the dephasing time of A^1_{1g} phonon is about 5.4 ps, and the dephasing time of A^2_{1g} phonon is much shorter, 0.72 ps. The possible reasons for stronger phonon damping observed experimentally are that more than one mode can be excited (see below) and also the existence of defects in the sample.

We now analyze the possible processes that drive phonon oscillations, specifically, the ponderomotive force, the thermal force, and the polarization force.[19] Since our sample has its c axis perpendicular to the sample surface, the ponderomotive force and the thermal force that originate from the electric

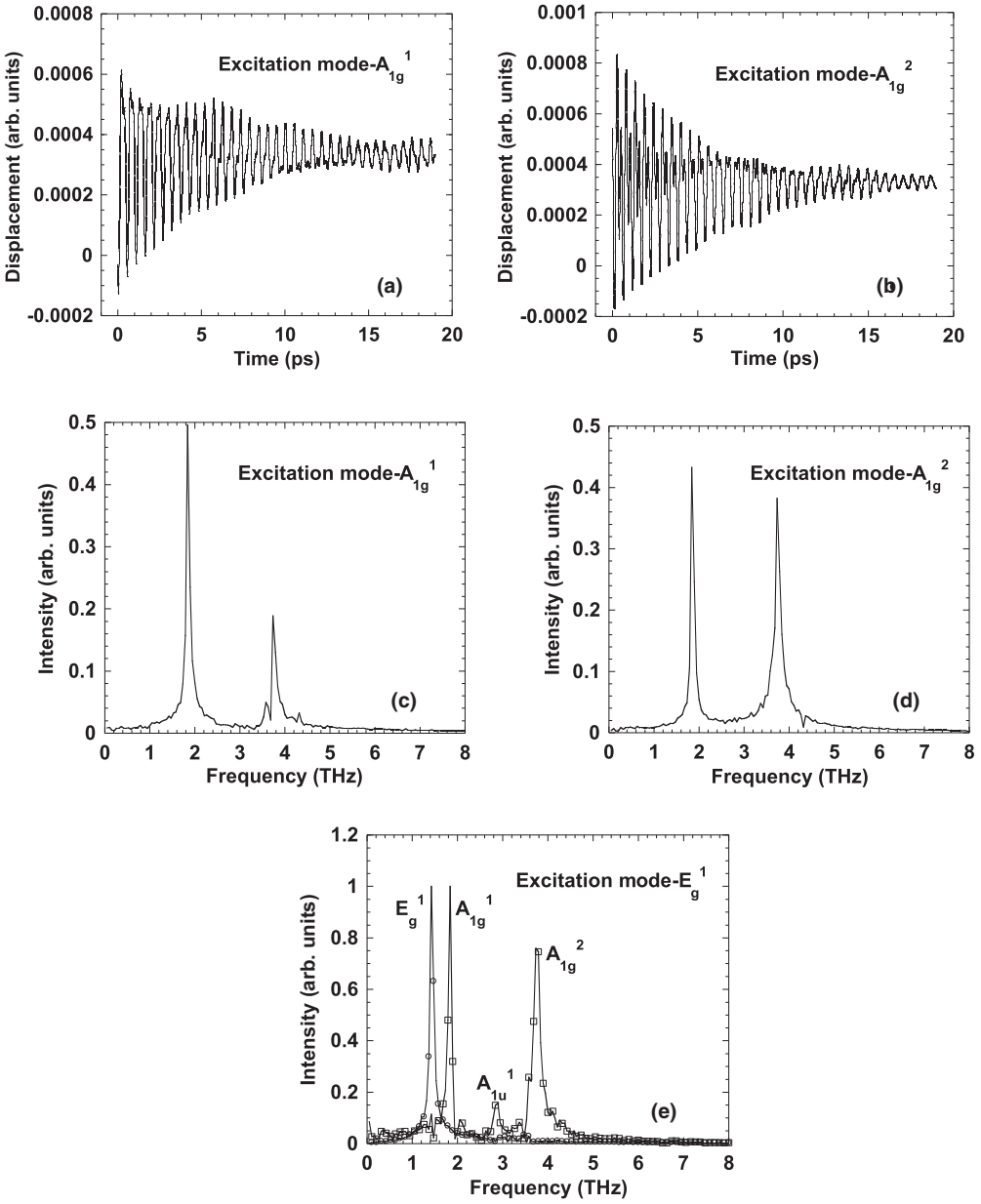

FIG. 3. Transient atomic displacements of TeI atoms with (a) A^1_{1g} excitation and (b) A^2_{1g} excitation. (c), (d) Corresponding FFT spectra for A^1_{1g} and A^2_{1g} excitation. (e) FFT spectra with E^1_g excitation.

field gradient and temperature gradient along the c axis can be responsible for generating the longitudinal A^1_{1g} and A^2_{1g} phonons. The ponderomotive force and the thermal force can be estimated as:[19]

$$f_{\text{pond}} \approx \frac{\varepsilon_D - 1}{\delta_s}\frac{I}{c} \quad , \quad f_{\text{thermal}} \approx \frac{n_e k_B T_{e,\max}}{\delta_s} \quad . \qquad (2)$$

For Bi_2Te_3, the Drude-type cross-plane dielectric constant ε_D is 12.81, calculated from the dielectric constant,[21] and the penetration depth is about 9.1 nm for the excitation wavelength of 400 nm. c is the speed of light, and k_B is the Boltzmann constant. The peak laser intensity is estimated as $I = F/t_p$, where F is the laser fluence and t_p is the pulse width (0.25 mJ/cm^2 and 100 fs). The hot electron density is estimated as $n_e = \alpha F/(\Delta E \delta_s)$, where α is the absorptivity (0.31 at 400 nm) and ΔE is the bandgap [0.15 eV for Bi_2Te_3 (see Ref. 21)]. Here avalanche excitation of electrons is assumed since the photon energy (3.1 eV) is much larger than the band gap. The value of n_e is determined to be 3.55×10^{27} m^{-3}, which is then used to evaluate the Fermi energy of the excited electrons, $\varepsilon_F = \hbar^2(3\pi^2 n_e)^{2/3}/(2m)$ (see Ref. 28), where m is the mass of electrons and $\hbar$ is the reduced Planck's constant. The value of ε_F is calculated to be 0.85 eV. The specific heat of the excited electrons is calculated as $c_v = \pi^2 k_B^2 T_e n_e/(2\varepsilon_F)$, where T_e is the electron temperature. The absorbed energy density by electrons is $\alpha F/\delta_s = \int_{T_0}^{T_{e,\max}} c_v dT$, where $T_{e,\max}$ and T_0 are the maximum temperature and the initial temperature, respectively. The maximum electron temperature $T_{e,\max}$ is then estimated as $T_{e,\max} = [4\varepsilon_F \alpha F/\pi^2 n_e \delta_s]^{1/2}/k_B$, where $T_{e,\max}$ is assumed to be much higher than T_0 and $T_{e,\max}$

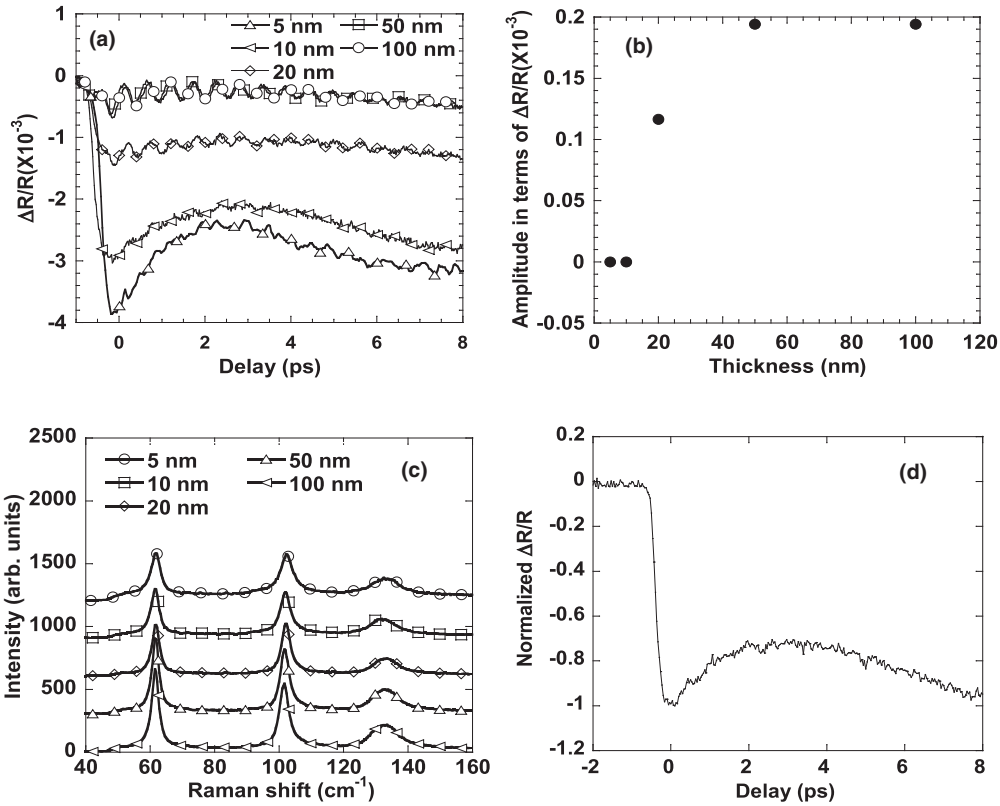

FIG. 4. (a) Coherent phonons in Bi_2Te_3 thin films with different thicknesses. (b) Coherent phonon amplitude versus the Bi_2Te_3 film thickness, obtained by fitting with a damped oscillator. (c) Raman spectra of Bi_2Te_3 thin films with different thicknesses. The three peaks are 62 cm^{-1} (1.86 THz), 102 cm^{-1} (3.06 THz), and 132 cm^{-1} (3.96 THz) for the A^1_{1g}, the E^2_g, and the A^2_{1g} modes. (d) Pump-probe signal of 10-nm-thick Bi_2Te_3 thin film illuminated by 30° incident pump beam.

is determined to be 2636 K. It is then found from Eq. (2) that in our case, the thermal force $f_{\text{thermal}} = 1.42 \times 10^{16} \text{N/m}^3$ dominates at the end of pump pulse, which is about two orders of magnitude higher than the ponderomotive force, $f_{\text{pond}} = 1.08 \times 10^{14} \text{N/m}^3$.

Both the thermal force and the ponderomotive force are gradient force, as they depend on either a thermal gradient or an electric-field gradient. On the other hand, we note that the gradient force does not produce the exact motion on Bi or Te ions of the A^1_{1g} or the A^2_{1g} mode as depicted in Fig. 1(a), rather, it produces a combination of the motions of the two modes. This indicates that these two modes can be excited simultaneously, which agrees with the experimental observation that there is no time delay between generations of the two phonon modes.

In our experiments, transverse phonons, which can be generated by the polarization force, are not observed since anisotropic detection[29] is not implemented. It is possible that the transverse modes are also generated but decay into the observed longitudinal phonons quickly. For example, the lifetime of the E_g mode is found to be short in Bi.[30] In addition, the excited carrier density in our case is similar to that used for Bi where strong phonon-phonon interaction is predicted.[5,31] The MD calculations also show that it is indeed possible that transverse phonons can generate longitudinal phonon modes. Figure 3(e) shows the phonon spectra if the initial excitation is the E^1_g mode. In this case, both A^1_{1g} and A^2_{1g} phonons are also generated. In addition, due to the asymmetrical Bi_2Te_3 lattice structure, the polarization force can directly excite the longitudinal phonon modes. The polarization force can be estimated as:[19]

$$f_{\text{polarization}} \approx \frac{4\pi \chi_0}{d} \frac{I}{c}, \tag{3}$$

where $\chi_0 \approx (\varepsilon_D - 1)/4\pi$ (see Ref. 32), and d is the averaged nearest-neighbor distance (~3.33 Å for Bi_2Te_3). The polarization force is estimated to be about $2.96 \times 10^{15} \text{N/m}^3$, larger than the ponderomotive force but smaller than the thermal force.

To evaluate the possibility that the observed A_{1g} modes are generated by initially excited E_g phonons or directly excited by the polarization force, experiments were carried out on samples with thinner thicknesses, from 100 nm to 5 nm. It is seen from Fig. 4(a) that while the oscillations in 100-nm- and 50-nm-thick films have similar amplitudes (also similar to the 1-μm film), the amplitude of coherent phonon decreases significantly when the film thickness decreases, and no coherent phonons can be observed when the thickness is 10 nm [Fig. 4(b)]. We verified that the thinner films still have crystalline structure, as shown in the Raman scattering data in Fig. 4(c). The widths of the Raman peaks in the thinner films are slightly wider, indicating longer interatomic distances or larger tensile stress and stronger anharmonicity in thinner films. The band gap in

the very thin Bi_2Te_3 films can be wider, for example, ~0.25 eV in 5-nm-thick films compared with 0.15 eV in bulk,[33] but still much smaller than the laser photon energy, so the light absorption process is still interband transition.

We attribute the sharp decrease of the phonon oscillations in 10-nm and 5-nm films to the lack of gradient force driving the phonon generation. This is because the optical absorption depth in Bi_2Te_3 is 9.1 nm at 400 nm wavelength. These result in a nearly uniform electric field across a thickness less than 10 nm. We also irradiate the pump pulse at an inclined angle with respect to the sample surface. The polarization force thus has a component along the *c* axis of the Bi_2Te_3 crystal. Figure 4(d) shows that similar to the results in Fig. 4(a), no coherent phonon oscillation is observed. This indicates that the polarization force is not sufficient to generate the observed longitudinal phonon modes. Therefore, we conclude that the longitudinal phonon modes observed in the experiments are not decayed from the E_g mode excitation or directly excited by the polarization force. An additional observation from Fig. 4(a) is that there is a large amplitude, slow varying reflectivity change. Measurements taken at longer time showed oscillations with period of 20 ps, regardless of the film thickness. Therefore, these oscillations can be different from the acoustic breathing modes whose oscillation periods are thickness dependent[34] and need to be further investigated.

The absence of coherent oscillations in the very thin films shows that a gradient force, such as the one produced by thermal force, is needed to drive the coherent phonon oscillation. This is in fact contradictory to the ISRS mechanism, which does not require a gradient in the excitation field. On the other hand, coherent phonon excitation by gradient force(s) should still follow the general picture of DECP, i.e., a sudden force field displaces ions out of their equilibrium positions, causing coherent phonon oscillations, which is a refined picture of phonon generation process within DECP.

In summary, we studied the coherent phonon dynamics in Bi_2Te_3 using ultrafast phonon spectroscopy and perturbation-based MD simulations. Complex features observed in phonon spectroscopy were determined to be the A^1_{1g} and the A^2_{1g} longitudinal phonon modes. Using thin films with thicknesses comparable or less than the optical absorption depth in combination with the MD analyses, it was found that the A_{1g} phonons were driven by gradient forces such as thermal force, which provides a refined picture of phonon generation process within DECP.

We would like to acknowledge the support by the National Science Foundation, the DARPA MESO program (N66001-11-1-4107), and the DARPA DSO program (ONR N00014-04-C-0042).

*Current address: Department of Mechanical Engineering, The University of Texas at Austin, Austin, Texas, 78712.
†These two authors contributed equally to this work.
‡Corresponding author: xxu@purdue.edu

[1] R. Venkatasubramanian, E. Siivola, T. Colpitts, and B. O'Quinn, Nature **413**, 597 (2001).
[2] H. Zhang, C. X. Liu, X. L. Qi, X. Dai, Z. Fang, and S. C. Zhang, Nat. Phys. **5**, 438 (2009).
[3] T. K. Cheng, J. Vidal, H. J. Zeiger, G. Dresselhaus, M. S. Dresselhaus, and E. P. Ippen, Appl. Phys. Lett. **59**, 1923 (1991).
[4] M. F. DeCamp, D. A. Reis, P. H. Bucksbaum, and R. Merlin, Phys. Rev. B **64**, 092301 (2001).
[5] M. Hase, M. Kitajima, S. Nakashima, and K. Mizoguchi, Phys. Rev. Lett. **88**, 067401 (2002).
[6] A. Q. Wu and X. Xu, Appl. Phys. Lett. **90**, 251111 (2007).
[7] M. Hase, K. Ishioka, J. Demsar, K. Ushida, and M. Kitajima, Phys. Rev. B **71**, 184301 (2005).
[8] G. C. Cho, W. Kütt, and H. Kurz, Phys. Rev. Lett. **65**, 764 (1990).
[9] Y. M. Chang, C. T. Chuang, C. T. Chia, K. T. Tsen, H. Lu, and W. J. Schaf, Appl. Phys. Lett. **85**, 5224 (2004).
[10] Y. Li, V. A. Stoica, L. Endicott, G. Wang, C. Uher, and R. Clarke, Appl. Phys. Lett. **97**, 171908 (2010).
[11] M. Hase, M. Katsuragawa, A. M. Constantinescu, and H. Petek, Nature Photon. **6**, 243 (2012).
[12] Y. Wang, X. Xu, and R. Venkatasubramanian, Appl. Phys. Lett. **93**, 113114 (2008).
[13] K. Kato, K. Oguri, A. Ishizawa, H. Nakano, and T. Sogawa, J. Appl. Phys. **111**, 113520 (2012).
[14] Y. Wang, X. Xu, and J. Yang, Phys. Rev. Lett. **102**, 175508 (2009).
[15] H. J. Zeiger, J. Vidal, T. K. Cheng, E. P. Ippen, G. Dresselhaus, and M. S. Dresselhaus, Phys. Rev. B **45**, 768 (1992).
[16] G. A. Garrett, T. F. Albrecht, J. F. Whitaker, and R. Merlin, Phys. Rev. Lett. **77**, 3661 (1996).
[17] T. E. Stevens, J. Kuhl, and R. Merlin, Phys. Rev. B **65**, 144304 (2002).
[18] D. Boschetto, E. G. Gamaly, A. V. Rode, B. Luther-Davies, D. Glijer, T. Garl, O. Albert, A. Rousse, and J. Etchepare, Phys. Rev. Lett. **100**, 027404 (2008).
[19] T. Garl, E. G. Gamaly, D. Boschetto, A. V. Rode, B. Luther-Davies, and A. Rousse, Phys. Rev. B **78**, 134302 (2008).
[20] R. Venkatasubramanian, T. Colpitts, E. Watko, M. Lamvik, and N. El-Masry, J. Cryst. Growth **170**, 817 (1997).
[21] D. L. Greenaway and G. Harbeke, J. Phys. Chem. Solids **26**, 1585 (1965).
[22] W. Richter, H. Köhler, and C. R. Becker, Phys. Status Solidi B **84**, 619 (1977).
[23] B. Qiu and X. Ruan, Phys. Rev. B **80**, 165203 (2009).
[24] Y. Wang, B. Qiu, A. J. H. McGaughey, X. Ruan, and X. Xu, J. Heat Transfer **135**, 091102 (2013).
[25] D. Wolf, P. Keblinski, S. R. Phillpot, and J. Eggebrecht, J. Chem. Phys. **110**, 8254 (1999).
[26] A. Q. Wu, X. Xu, and R. Venkatasubramanian, Appl. Phys. Lett. **92**, 011108 (2008).
[27] W. Kullmann, J. Geurts, W. Richter, N. Lehner, H. Rauh, U. Steigenberger, G. Eichhorn, and R. Geick, Phys. Status Solidi B **125**, 131 (1984).
[28] N. W. Ashcroft and N. D. Mermin, *Solid State Physics* (W. B. Saunders, Philadelphia, 1976).
[29] T. Dekorsy, H. Auer, C. Waschke, H. J. Bakker, H. G. Roskos, and H. Kurz, Phys. Rev. Lett. **74**, 738 (1995).

[30] J. J. Li, J. Chen, D. A. Reis, S. Fahy, and R. Merlin, Phys. Rev. Lett. **110**, 047401 (2013).
[31] E. S. Zijlstra, L. L. Tatarinova, and M. E. Garcia, Phys. Rev. B **74**, 220301(R) (2006).
[32] C. Kittel, *Introduction to Solid State Physics* (John Wiley & Sons, Inc., New York, 1976).
[33] Y.-Y. Li, G. Wang, X.-G. Zhu, M.-H. Liu, C. Ye, X. Chen, Y.-Y. Wang, K. He, L.-L. Wang, X.-C. Ma, H.-J. Zhang, X. Dai, Z. Fang, X.-C. Xie, Y. Liu, X.-L. Qi, J.-F. Jia, S.-C. Zhang, and Q.-K. Xue, Adv. Mater. **22**, 4002 (2010).
[34] S. Nie, X. Wang, H. Park, R. Clinite, and J. Cao, Phys. Rev. Lett. **96**, 025901 (2006).